Macromolecules

Article

pubs.acs.org/Macromolecules

Thiol–Ene Elastomers Derived from Biobased Phenolic Acids with Varying Functionality

Guozhen Yang,[†] Samantha L. Kristufek,[‡] Lauren A. Link,[‡] Karen L. Wooley,[‡] and Megan L. Robertson*[,†]

[†]Department of Chemical and Biomolecular Engineering, University of Houston, Houston, Texas 77204-4004, United States

[‡]Department of Chemistry, Department of Chemical Engineering, Department of Materials Science & Engineering, Texas A&M University, College Station, Texas 77842-3012, United States

Supporting Information

ABSTRACT: The synthesis and physical properties of thiol–ene elastomers derived from plant-based phenolic acids were explored. Phenolic acids of varying functionality (ranging from 2 to 4 hydroxyl and carboxyl groups per molecule) and relative placement of functional groups (*ortho*, *meta*, *para*) were allylated and subsequently reacted with a multifunctional thiol using a photoinitiator. The thermal and mechanical behaviors of the resulting elastomers were characterized. The networks derived from difunctional allylated phenolic acids exhibited narrow glass transitions (indicating a high degree of network homogeneity) and glass transition temperatures (T_g) which correlated with their cross-link density. The *para* placement of allyl groups on the allylated phenolic acid produced a network with the highest cross-link density, T_g, modulus, tensile strength, and elongation at break (followed by *ortho* and then *meta*). As the functionality of the allylated monomer increased (to 3–4 allyl groups per molecule), the cross-link density remained high yet the T_g decreased, attributed to a lower concentration of benzene rings throughout the network structure (as all networks were prepared at the stoichiometric ratio of allyl and thiol functional groups). The networks derived from the higher functionality allylated phenolic acids also exhibited lower elongation at break and associated tensile strength and tensile toughness, likely due to increased heterogeneity of the networks (indicated by higher glass transition widths compared to the networks derived from difunctional allylated phenolic acids). All networks exhibited behavior consistent with an ideal elastomer (affine network) at low to moderate strains, albeit with lower moduli than predicted from the monomer chemical structure. At the high end of the strain ranges achieved, some of the networks exhibited strain hardening behavior. This work develops fundamental relationships between the molecular structure of the phenolic acids, including number and placement of functional groups, and the physical properties of the resulting networks.

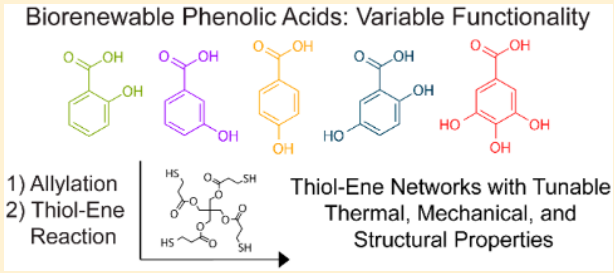

INTRODUCTION

The development of sustainable feedstocks to replace petroleum for the derivation of polymers has been a subject of much recent interest in academia and industry.[1,2] Thiol–ene elastomers, which are traditionally derived from petrochemical-based thiol- and ene-containing monomers, are attractive materials for coatings and adhesives[3] due to their ease of fabrication, low shrinkage and stress,[4] and high degree of network homogeneity[3,5−7] relative to other elastomeric materials. The thiol–ene chemistry employed to synthesize these elastomeric films has many advantageous features including high conversion and yield, rapid reaction rates, solvent-free conditions, lack of water and oxygen sensitivity, lack of byproducts, and ability to impart spatial and temporal control over the reaction (in the case of photoinitiation).[3,5] A diverse array of ene- and thiol-bearing molecules have been investigated for the preparation of thiol–ene networks,[3,5,6] though they are predominantly derived from petroleum sources. Biorenewable molecules are attractive replacements for the components of thiol–ene elastomers as mild reaction conditions are employed, and the ability to conduct solvent-free syntheses enhances their environmental benefit. Relatively few studies have reported the derivation of thiol–ene elastomeric films using biorenewable components; some notable examples include the use of vegetable oils and their fatty acids,[8−12] carbohydrates,[13,14] terpenes,[15] and other plant-derived molecules.[16,17]

Here, we report on the utilization of plant-based phenolic acids as the ene-containing components of thiol–ene networks. Phenolic acids are plant metabolites widely distributed in nature.[18−21] They are often found in plant byproducts including the skins and seeds of fruits and vegetables.[18−21] Phenolic acids offer many advantages as biorenewable monomers: their rigid aromatic rings are expected to provide mechanical strength to the resulting polymers, and the presence of multiple hydroxyl groups and carboxyl groups leads to ease of functionalization.

Received: May 15, 2016
Revised: August 16, 2016
Published: October 5, 2016

DOI: 10.1021/acs.macromol.6b01018
Macromolecules 2016, 49, 7737−7748

Through the choice of phenolic acid, the number and relative placement of hydroxyl and carboxyl groups can be varied, which is expected to be a convenient method of tuning the physical properties of the resulting polymers. We have investigated five allylated phenolic acids as components of thiol−ene networks: difunctional molecules with varying placement of functional groups (*ortho*, *meta*, and *para*) and molecules with varying number of functional groups (ranging from 2 to 4). This work extends an earlier publication which compared the behavior of thiol−ene networks derived from the difunctional *o*- and *p*-hydroxybenzoic acids;[22] herein we include the *m*-hydroxybenzoic acid as well as the tri- and tetrafunctional phenolic acids. The thermal, mechanical, and structural properties of the thiol−ene networks were investigated. This work develops fundamental relationships between the functionality of the phenolic acids (number and placement of functional groups) and the physical properties of the resulting networks, providing new insight into the tailored design of biorenewable monomers for thiol−ene networks. Gaining such knowledge is an important first step toward the widespread implementation of biobased molecules in thiol−ene network applications.

EXPERIMENTAL DETAILS

Materials. All chemicals were purchased from Sigma-Aldrich unless otherwise noted below. Five phenolic acids were used in this study: salicylic acid (SA, ≥99%, FG/Halal/Kosher), 4-hydroxybenzoic acid (4HBA, 99%, ReagentPlus), 3-hydroxybenzoic acid (3HBA, 99%, ReagentPlus), gentisic acid (GenA, 98%), and gallic acid (GalA, 97.5−102.5% by titration). The chemical structures of all phenolic acids are shown in Figure 1.

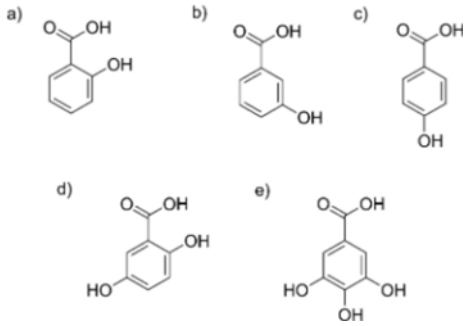

Figure 1. Chemical structures of phenolic acids used in this study: (a) salicylic acid (SA), (b) 3-hydroxybenzoic acid (3HBA), (c) 4-hydroxybenzoic acid (4HBA), (d) gentisic acid (GenA), (e) gallic acid (GalA).

Nuclear Magnetic Resonance (NMR). The following NMR experiments were performed on a JEOL ECA-400 instrument using deuterated dimethyl sulfoxide (Cambridge Isotope Laboratories, Inc., 99.9% D) as the solvent: ^{1}H NMR (400 MHz), ^{13}C NMR (100 MHz), DEPT 45, 90, 135, COSY, HSQC, and HMBC. Chemical shifts were referenced to the solvent proton resonance (2.5 ppm). Spectra obtained from allylated SA (aSA) and allylated 4HBA (a4HBA) have been previously reported in ref 22. Spectra obtained on 3HBA, GenA, GalA, allylated 3HBA (a3HBA), allylated GenA (aGenA), and allylated GalA (aGalA) are included in the Supporting Information (Figures S1−S6).

Fourier Transform Infrared Spectroscopy (FTIR). FTIR spectra were recorded on a Thermo Scientific Nicolet 4700 spectrometer in transmission mode as well as using an attenuated total reflection (ATR) stage (containing a germanium crystal). The OMNIC Series software was used to follow selected peaks at 1.928 cm^{-1} resolution using 32 scans. FTIR spectra were collected on allylated monomers and thiol−ene networks (prior to exposure of the sample with UV, and after 15 and 30 min of UV exposure, and 30 min of isothermal curing at 150 °C). FTIR spectra are included in the Supporting Information (Figure S7).

Monomer Synthesis. Allylation of the phenolic acids was conducted following literature procedures.[22,23] Phenolic acid (10 g) was dissolved into 340 mL of *N*,*N*-dimethylformamide (DMF, BDH, ≥99.8%, ACS reagent) in a 1000 mL glass round-bottom flask equipped with a rubber septum and a magnetic stirring bar. The temperature was maintained at 0 °C using an ice bath. Potassium carbonate (K_2CO_3, ≥99.0%, ACS reagent) was added to the flask. The molar ratio of K_2CO_3 to phenolic acid was 2.20 to 1.00 (for 3HBA), 3.30 to 1.00 (for GenA), and 4.40 to 1.00 (for GalA). After 3 min of stirring, allyl bromide (97%) was added dropwise with a syringe (the molar ratio of allyl bromide to phenolic acid was 2.20 to 1.00 (for 3HBA), 3.30 to 1.00 (for GenA), and 4.40 to 1.00 (for GalA)). The solution was stirred at room temperature for 48 h. Next, 340 mL of distilled water was added into the solution. The solution was mixed with an equivalent volume of ethyl acetate (BDH, ≥99.5%, ACS grade), and a separatory funnel was used to recover the ethyl acetate phase which contained the product. The remaining aqueous phase was extracted two additional times with ethyl acetate (the volume of ethyl acetate was equal to the aqueous phase volume in each extraction). The organic phase containing the allylated phenolic acid was washed with an equivalent volume of saturated brine and purified through drying with magnesium sulfate (BDH, ≥99.0%, anhydrous reagent grade) followed by distillation using a rotary evaporator to remove ethyl acetate. DMF was removed from the allylated phenolic acid through drying in a vacuum oven at 50 °C, until the NMR peaks associated with DMF (7.96, 2.94, and 2.78 ppm) were not observed. NMR and FTIR spectra obtained on SA, 4HBA, aSA, and a4HBA have been previously reported in ref 22.

3-Hydroxybenzoic Acid (3HBA). ^{1}H NMR (400 MHz, DMSO-d_6, ppm): δ 12.74 (broad s, 1H), 9.75 (broad s, 1H), 7.33 (d, J = 7.56 Hz, 1H), 7.29 (s, 1H), 7.24 (t, J = 7.56 Hz, 1H), 6.95 (d, J = 7.56 Hz, 1H). ^{13}C NMR (100 MHz; DMSO-d_6, ppm): δ 167.9, 157.9, 132.6, 130.1, 120.5, 120.4, 116.3.

Allyl 3-Allyloxybenzoate. (allylated 3HBA is referred to as "a3HBA" in this article). ^{1}H NMR (400 MHz, DMSO-d_6, ppm): δ 7.54 (ddd, J = 7.79, 1.37, 1.37 Hz, 1H), 7.44 (dd, J = 2.75, 1.83 Hz, 1H), 7.42 (dd, J = 7.79, 7.79 Hz, 1H), 7.23 (ddd, J = 8.24, 2.75, 0.92 Hz, 1H), 6.06−5.96 (m, 2H), 5.40−5.34 (m, 2H), 5.24 (ddt, J = 10.53, 1.37, 1.37 Hz, 2H), 4.77 (ddd, J = 5.50, 1.37, 1.37 Hz, 2H), 4.61 (ddd, J = 5.04, 1.37, 1.37 Hz, 2H). ^{13}C NMR (100 MHz; DMSO-d_6, ppm): δ 165.7, 158.8, 133.9, 133.1, 131.4, 130.6, 122.1, 120.6, 118.5, 118.1, 115.2, 68.9, 65.7. FTIR (ATR): 3082, 2943, 2877, 1720, 1649, 1599, 1585, 1487, 1443, 1424, 1361, 1319, 1291, 1272, 1213, 1158, 1107, 1078, 1027, 993, 983, 928, 875, 809, 754, 682, 640 cm^{-1}.

Gentisic Acid (GenA). ^{1}H NMR (400 MHz, DMSO-d_6, ppm): δ 13.75 (broad s, 1H), 10.65 (broad s, 1H), 9.13 (s, 1H), 7.11 (d, J = 2.93 Hz, 1H), 6.92 (dd, J = 8.79, 2.93 Hz, 1H), 6.75 (d, J = 8.79 Hz, 1H). ^{13}C NMR (100 MHz; DMSO-d_6, ppm): δ 172.3, 154.6, 149.9, 124.3, 118.3, 115.0, 113.1.

Allyl 2,5-Bis(allyloxy)benzoate. (allylated GenA is referred to as "aGenA" in this article). ^{1}H NMR (400 MHz, DMSO-d_6, ppm): δ 7.18 (d, J = 2.93 Hz, 1H), 7.10 (dd, J = 8.79, 2.93 Hz, 1H), 7.05 (d, J = 8.79 Hz, 1H), 6.03−5.92 (m, 3H), 5.43−5.32 (m, 3H), 5.23−5.17 (m, 3H), 4.71 (ddd, J = 5.37, 1.47, 1.47 Hz, 2H), 4.54−4.50 (m, 4H). ^{13}C NMR (100 MHz; DMSO-d_6, ppm): δ 165.7, 152.1, 151.8, 134.2, 134.0, 133.1, 121.5, 120.3, 118.3, 118.0, 117.4, 116.8, 116.3, 70.0, 69.3, 65.5. FTIR (ATR): 3084, 3020, 2987, 2946, 2880, 1729, 1705, 1648, 1612, 1581, 1559, 1497, 1455, 1421, 1360, 1281, 1237, 1201, 1156, 1105, 1066, 1025, 996, 926, 892, 810, 780 cm^{-1}.

Gallic Acid (GalA). ^{1}H NMR (400 MHz, DMSO-d_6, ppm): δ 12.22 (s, 1H), 9.17 (s, 2H), 8.82 (s, 1H), 6.88 (s, 2H). ^{13}C NMR (100 MHz; DMSO-d_6, ppm): δ 168.0, 145.9, 138.5, 120.9, 109.2.

Allyl 3,4,5-Tris(allyloxy)benzoate. (allylated GalA is referred to as "aGalA" in this article). ^{1}H NMR (400 MHz, DMSO-d_6, ppm): δ 7.21 (s, 2H), 6.07−5.93 (m, 4H), 5.41−5.22 (m, 7H), 5.14 (ddt, J = 10.5, 1.47, 1.47 Hz, 1H), 4.75 (ddd, J = 5.37, 1.47, 1.47 Hz, 2H), 4.61 (ddd,

DOI: 10.1021/acs.macromol.6b01018
Macromolecules 2016, 49, 7737−7748

J = 4.88, 1.47, 1.47 Hz, 4H), 4.51 (ddd, J = 5.86, 1.47, 1.47 Hz, 2H). ^{13}C NMR (100 MHz, DMSO-d_6, ppm): δ 165.4, 152.4, 141.6, 134.9, 134.0, 133.2, 125.1, 118.4, 118.0, 117.8, 108.4, 73.7, 69.9, 65.7. FTIR (ATR): 3080, 3021, 2985, 2945, 2871, 1716, 1648, 1586, 1498, 1455, 1422, 1375, 1362, 1328, 1290, 1264, 1236, 1204, 1130, 1109, 986, 926, 863, 812, 764 cm^{-1}.

Polymer Synthesis. UV curing of thiol−ene networks followed procedures similar to those reported in ref 16 and has been previously reported by our group for UV curing of aSA and a4HBA in ref 22. The allylated phenolic acid was mixed with pentaerythritol tetrakis(3-mercaptopropionate) (PETMP, >95%) (stoichiometry based on equal molar functional groups) and 1 wt % of the photoinitiator 2,2-dimethoxy-2-phenylacetophenone (DMPA, 99%) at room temperature in a 20 mL vial (using magnetic stirring), which was covered by aluminum foil. The mixture was placed in the following sample holders appropriate for each characterization experiment: (a) between two glass slides with a 0.4 mm glass spacer for TGA, DSC, DMA, and ATR-FTIR, (b) between two NaCl windows (32 mm diameter, 3 mm thick) with a 0.05 mm Teflon spacer for transmission-mode FTIR, and (c) in a Teflon dogbone-shaped mold following ASTM D638 (bar type 5, thickness 0.4 mm) for tensile testing. The sample was exposed under continuous 365 nm UV light (4 W, Spectroline ENF-240C) for 15 min and transferred to a convection oven at 150 °C for a specified period of time, summarized in Table 1. FTIR spectra obtained on networks synthesized from allylated SA and allylated 4HBA were reported in ref 22.

Table 1. Composition and Curing Protocol of Thiol−Ene Networks

allylated phenolic acid[a]	molar ratio of reagents (allylated phenolic acid: PETMP:photoinitiator)	UV exposure time/ isothermal postcuring time at 150 °C
aSA	1.0:0.50:0.018	15 min/10 min
a3HBA	1.0:0.50:0.018	15 min/10 min
a4HBA	1.0:0.50:0.018	15 min/10 min
aGenA	1.0:0.75:0.025	15 min/20 min
aGalA	1.0:1.0:0.032	15 min/20 min

[a]The phenolic acids were allylated and subsequently cured with pentaerythritol tetrakis(3-mercaptopropionate) (PETMP) and a photoinitiator, as described in the Experimental Details.

Network Synthesized from A3HBA. FTIR (ATR): 2922, 2852, 1737, 1716, 1600, 1584, 1488, 1469, 1443, 1387, 1352, 1320, 1275, 1225, 1140, 1106, 1074, 1033, 997, 937, 886, 808, 756, 683 cm^{-1}.

Network Synthesized from AGenA. FTIR (ATR): 2917, 2849, 1736, 1609, 1580, 1541, 1498, 1467, 1423, 1388, 1353, 1284, 1239, 1202, 1144, 1031, 930, 817, 784, 766, 746 cm^{-1}.

Network Synthesized from AGalA. FTIR (ATR): 2916, 2849, 1737, 1647, 1586, 1499, 1469, 1429, 1387, 1355, 1332, 1288, 1207, 1145, 1114, 1052, 1015, 931, 871, 843, 766 cm^{-1}.

Dynamic Mechanical Analysis (DMA). The dynamic mechanical behavior of cured thiol−ene films (following the protocol in the Polymer Synthesis section) was probed using a Q800 dynamic mechanical analyzer (TA Instruments) with a nitrogen environment. Specimens of 0.4 mm thickness were cut with a razor blade to have the following dimensions: 10 mm × 5 mm × 0.4 mm (length × width × thickness).

Four experiments and analyses were conducted: (1) isothermal strain sweeps were conducted at desired temperatures and using a frequency of 1 Hz to locate the range of strains in the linear viscoelastic region; (2) isothermal frequency sweeps were conducted from 0.1 to 10 Hz at desired temperatures, using a strain within the linear viscoelastic region; (3) time−temperature superposition of the data was performed at −10, −5, 0, 5, 10, 15, 20, 30, and 40 °C; and (4) temperature ramps were conducted at a constant strain and frequency. In the case of time−temperature superposition, the master curve was prepared using the TA Instruments Rheology Advantage Data Analysis software with 30 °C chosen as the reference temperature.

Differential Scanning Calorimetry (DSC). The glass transition temperature (T_g) was measured through DSC experiments conducted using a TA Instruments Q2000 calorimeter, calibrated with an indium standard, with a nitrogen flow rate of 50 mL/min. The cured sample (following the protocol in the Polymer Synthesis section) was placed in the calorimeter (using a Tzero aluminum pan), equilibrated at 40 °C, cooled to −40 C at a rate of 10 °C/min, and heated to 40 °C at a rate of 10 °C/min. The cooling and heating scans were repeated for a total of two measurements. The value of the T_g was determined using the half extrapolated tangents method in the Universal Analysis software.[24] The onset and endset temperatures were also identified with the Universal Analysis software.

Thermogravimetric Analysis (TGA). TGA experiments were conducted with a TA Instruments Q500 analyzer. The sample was cured following the protocol in the Polymer Synthesis section and transferred to the analyzer. The cured sample was heated from 30 to 800 °C at a rate of 10 °C/min in an argon environment (the balance argon purge flow was 40 mL/min and the sample purge flow was 60 mL/min).

Tensile Testing. Tensile testing was carried out with an Instron 5966 universal testing system containing a 2 kN load cell. Dogbone-shaped testing bars (ASTM D638, bar type 5, thickness 0.4 mm) were prepared following the procedure in the Polymer Synthesis section. Pneumatic grips (maximum force 2 kN) were used to affix the sample in the testing frame, at a compressed air pressure of 40 psi. The force and change in length were measured as the sample was elongated at a rate of 10 mm/min. Each measurement was repeated with five test specimens that broke in the gauge region and did not contain a visible defect at the point of fracture.

Density Measurement. The densities of phenolic acid-based thiol−ene networks were measured in a vial containing a calcium nitrate water solution of known concentration at room temperature. The water content was adjusted to determine the composition range over which the polymer transitioned from being suspended in the solvent to sinking in the solvent. This range was narrowed until the density could be determined to 2 significant digits after the decimal point. The exact density of calcium nitrate solution was determined through the quadratic equation fitting to the density−concentration data in a previous study.[25] The resulting densities were as follows: aSA-based thiol−ene networks, 1.22 g/mL; a3HBA-based thiol−ene networks, 1.22 g/mL; a4HBA-based thiol−ene networks, 1.22 g/mL; aGenA-based thiol−ene networks, 1.22 g/mL; aGalA-based thiol−ene networks, 1.22 g/mL.

RESULTS AND DISCUSSION

Synthesis of Thiol−Ene Networks Derived from Phenolic Acids. Five phenolic acids were explored as components of thiol−ene networks: SA, 3HBA, and 4HBA (difunctional phenolic acids with *ortho*, *meta*, and *para* placements of functional groups, respectively); GenA (a trifunctional phenolic acid); and GalA (a tetrafunctional phenolic acid). Allylation of the phenolic acids was conducted following procedures previously reported by our group,[22] also following a prior literature study.[23] Figure 2 shows the allylated versions of each phenolic acid.

NMR was used to monitor the progress of the allylation reaction (Figure 3 and Figures S1−S6; data obtained on aSA and a4HBA were discussed in ref 22), which are agreement with prior literature.[26−31] The ^{1}H NMR spectra of all allylated phenolic acids show the disappearance of peaks located in the range of 8−14 ppm associated with the carboxyl and hydroxyl groups in the phenolic acids. The peaks located in the region of 4−6 ppm correspond to the allyl groups in the allylated phenolic acids. The ratios of the peak area associated with the CH_2−O protons on the allyl group to the peak area associated with the aromatic protons are very close to the theoretical predictions (Table 2). The conversions of the allylation

DOI: 10.1021/acs.macromol.6b01018
Macromolecules 2016, 49, 7737−7748

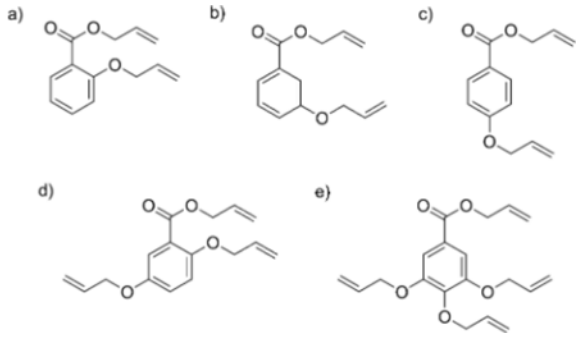

Figure 2. Chemical structures of allylated phenolic acids used to prepare thiol−ene networks: (a) aSA, (b) a3HBA, (c) a4HBA, (d) aGenA, and (e) aGalA.

reactions were quite high, 97−100% (Table 2), calculated using the integrals of peaks associated with aromatic protons of ^{1}H NMR data obtained on the allylated phenolic acids prior to extraction (reported in Figures S2, S4, and S6). The yields of allylated phenolic acids were around 80% (Table 2). The relative number and placement of functional groups on the phenolic acids did not have a significant impact on the allylation reaction, as evidenced by similar conversions and yields in all five phenolic acids (Table 2 and ref 22).

The photoinitiated thiol−ene reaction between the allylated phenolic acids and the tetrafunctional thiol PETMP (Scheme 1 and Scheme S1), which follows the well-established step-growth radical mechanism,[3,5] was monitored through FTIR. Allyl ethers generally exhibit high reactivities in the thiol−ene reaction,[3] and thiol−allyl ether systems exhibit high propagation rates relative to rates of chain transfer.[32]

FTIR spectra obtained upon UV curing of the allylated phenolic acids with the multifunctional thiol PETMP are shown in Figure S7 for a3HBA, aGenA, and aGalA and were previously reported in ref 22 for aSA and a4HBA (assignment of vibrational modes is summarized in Table S1). In all spectra, conversion of the thiol was monitored through disappearance of the peak located at 2570 cm^{-1} (S−H stretching), quantified in Tables S2−S6, while network formation was observed through an increase in the intensity of the peak located at 2950 cm^{-1} (alkane C−H stretching). Conversion of allyl groups on the allylated phenolic acids was monitored by decreases in the following peak intensities over time: 932 and 996 cm^{-1} (olefinic =C−H bending), 1647 cm^{-1} (C=C stretching), and 3080 cm^{-1} (olefinic =C−H stretching). We could not determine whether the peaks associated with the allyl groups disappeared completely, as they were all located in the vicinity of neighboring peaks (Figure S7). The peak located at 932 cm^{-1} may also include contributions from C−O stretching of ester groups present in both the phenolic acids and PETMP.[33,34] As increasing the UV exposure time beyond 15 min did not result in any appreciable differences in the FTIR spectra or conversion (Tables S2−S6), 15 min was chosen as the UV exposure time for all allylated phenolic acids (Table 1).

FTIR and differential scanning calorimetry (DSC) were employed to identify the isothermal annealing time for the thiol−ene networks following UV exposure to achieve the highest possible conversion of functional groups. Thiol−ene networks were prepared through 15 min of exposure to UV followed by isothermal curing in a convection oven at 150 °C (the reaction conversion increased after the 150 °C postcure, detailed in Tables S2−S6). In Figures S8 and S9, the maximum

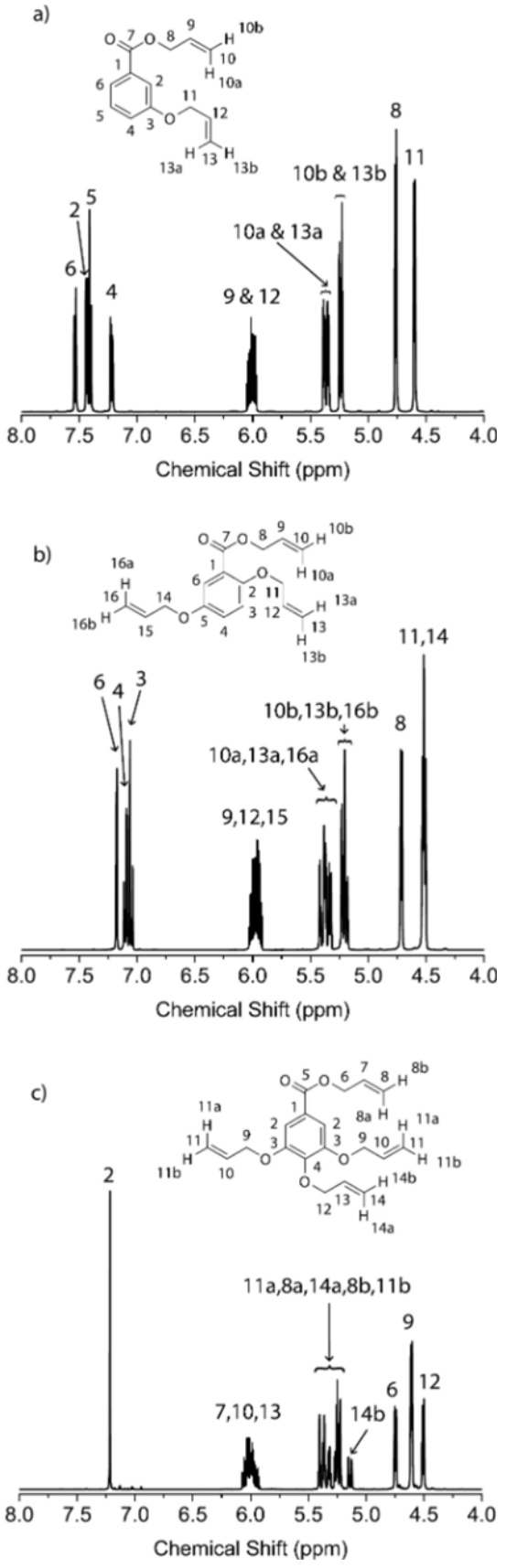

Figure 3. ^{1}H NMR data obtained from (a) a3HBA, (b) aGenA, and (c) aGalA. Additional spectra are included in Figures S1−S6. Spectra obtained from aSA and a4HBA were previously reported in ref 22.

DOI: 10.1021/acs.macromol.6b01018
Macromolecules 2016, 49, 7737−7748

Table 2. ^{1}H NMR Characterization of Phenolic Acid Allylation

phenolic acid	conv (%)	peak area of CH_2O on allyl group:peak area of aromatic protons[a]	yield (%)
3HBA	99.4	4.12:4.00 (4:4)	77
GenA	97.5	6.06:3.00 (6:3)	78
GalA	100	8.10:2.00 (8:2)	80

[a]Theoretical ratio is given in parentheses.

absorbance of various FTIR peaks and T_g are plotted as functions of the isothermal annealing time. For the networks derived from difunctional allylated phenolic acids (aSA, a3HBA, and a4HBA), the conversion and T_g did not change upon increasing the isothermal annealing time beyond 10 min, and therefore an isothermal annealing time of 10 min was chosen. In the case of networks derived from multifunctional allylated phenolic acids (aGenA and aGalA), a slightly longer isothermal annealing time of 20 min was chosen (to ensure the maximum possible conversion of functional groups, which did not change for annealing times beyond 20 min). The UV and isothermal curing protocols are summarized in Table 1. The final conversion of all networks following UV curing and isothermal annealing is reported in Table S7; the aSA network exhibited the highest conversion (97%), followed by the a3HBA, a4HBA, and aGenA networks (88%), with the lowest conversion achieved by the aGalA network (83%). The allyl ester and allyl ether moieties are anticipated to exhibit slightly different reactivities (increasing the electron density of the ene component increases the thiol−ene reaction rate;[3] the allyl ether has a higher electron density than the allyl ester[35]), and therefore it is more likely that unreacted allyl groups are associated with an ester rather than an ether. Increasing the UV exposure time and isothermal annealing time did not increase the conversion of any of the thiol−ene networks reported here. The inability to achieve 100% conversion in these networks is likely due to trapped functional groups (allyl and thiol) in the network at relatively high conversion.

We quantified the biorenewable content in the thiol−ene networks by calculating the wt % of phenolic acid in the final material. The biorenewable content (i.e., the contribution of the phenolic acids, which can be derived from plant sources) of the aSA and a4HBA networks, both derived from difunctional allylated phenolic acids, is calculated to be 29 wt % (SA is found in various fruits and vegetables,[36] including their waste products, and 4HBA is found in coconut husks[37]). We do not consider a3HBA to be a biorenewable chemical, as there is not a significant plant-based source for 3HBA to our knowledge. Rather, we have included this chemical in this study to highlight observed trends in the physical properties of the thiol−ene networks derived from difunctional phenolic acids, in which the relative placement of functional groups is varying (3HBA is the *m*-hydroxybenzoic acid, complementing SA and 4HBA, which are respectively *o*- and *p*-hydroxybenzoic acids). The biorenewable contents of the aGenA and aGalA networks (derived from tri- and tetrafunctional allylated phenolic acids) are calculated to be 23 and 20 wt %, respectively (GenA is one of the most commonly found aromatic acids in plants,[38] in both edible and nonedible components, and GalA is found in plant sources such as bark, leaves, and nuts[39]). We conducted similar calculations for prior literature studies which report thiol−ene networks derived from biorenewable components and found that the biorenewable content in prior studies on thiol−ene networks ranged from 20 to 58 wt %.[8−10,12−16] One strategy to increase the total biorenewable content in our materials would be to employ a multifunctional thiol derived from a renewable resources,[10,17] in addition to the allylated phenolic acids.

Physical Properties of Thiol−Ene Networks Derived from Phenolic Acids of Varying Functionality. Dynamic mechanical analysis (DMA) was used to explore the dynamic moduli of the thiol−ene networks. The strain and frequency dependencies of the storage (E') and loss (E'') moduli are shown in Figures S10 and S11 at selected temperatures. Time−temperature superposition was applied to the frequency-dependent E' and E''. Reduced moduli (E'_r and E''_r) were first obtained by multiplying each modulus by a vertical shift factor, b_T:[40,41]

$$b_T = \frac{T_0}{T} \tag{1}$$

$$E'_r = b_T E' \tag{2}$$

$$E''_r = b_T E'' \tag{3}$$

where the reference temperature, T_0, was taken to be 30 °C. The reduced moduli were then shifted horizontally by applying a horizontal shift factor, a_T, at each temperature:

$$\omega_r = a_T \omega \tag{4}$$

where ω_r are the reduced frequencies. At each temperature, a_T was identified as that required to produce a smooth and continuous master curve. The master curves containing the shifted data are shown in Figure 4.

The Williams−Landel−Ferry (WLF) equation is well-established for describing the temperature dependence of a_T for polymers at temperatures above or in the vicinity of the T_g:[42]

$$\log a_T = \frac{-C_1(T - T_0)}{C_2 + (T - T_0)} \tag{5}$$

The WLF equation fit to the shift factor as a function of temperature is shown in Figure 5. In all networks, the data are consistent with the WLF equation. C_1 is an empirical

Scheme 1. Photoinitated Thiol−Ene Reaction between a3HBA and the Tetrafunctional Thiol PETMP[a]

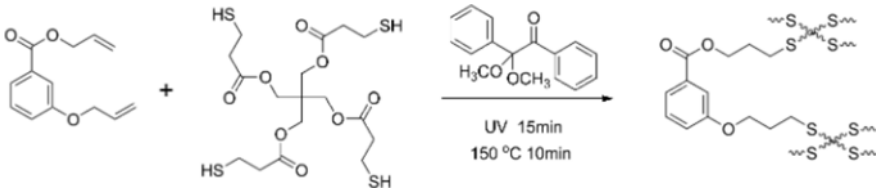

[a]Equivalent thiol−ene reactions for the other allylated phenolic acids (aSA, a4HBA, aGenA, and aGalA) are shown in Scheme S1.

DOI: 10.1021/acs.macromol.6b01018
Macromolecules 2016, 49, 7737−7748

parameter; however, C_2 can be described as $C_2 = f_r/\alpha_f$, where f_r is the fractional free volume of the material at the reference temperature and α_f is the coefficient of thermal expansion of the free volume ($\alpha_f \sim \alpha_l - \alpha_g$, where α_l and α_g are the coefficients of expansion of the liquid and glassy states, respectively). Significant differences are observed in the C_2 values for all five networks, possibly indicating differences in the values of f_r and α_f for these materials.

The cross-link density (υ_c) of each thiol−ene network was calculated from E' in the rubbery plateau region of the plot of E' vs ω (Figure S11), using the theory of rubber elasticity:[43]

$$\upsilon_c = \frac{E'}{3RT} \tag{6}$$

where R is the gas constant. The resulting cross-link densities are summarized in Tables S8−S12, in which measurements were obtained on multiple specimens over multiple independently prepared specimens for each type of thiol−ene network. Figure 6a shows the resulting average values of the cross-link densities for the thiol−ene networks of varying functionality. The cross-link densities (and also plateau moduli) of the thiol−ene networks prepared from the difunctional aSA and a3HBA (*ortho* and *meta* placements of allyl groups, respectively) were quite similar to one another. A significant increase in cross-link density was observed for the thiol−ene network prepared from the difuctional a4HBA (*para* placement of allyl groups). We previously proposed that the lower cross-link density of the aSA network as compared to the a4HBA network is due to the neighboring allyl groups found on aSA; the structure of the aSA network contains bulky aromatic groups intruded into network, which impacts the networks architecture and reduces the cross-link density.[22] Surprisingly, we see that the *ortho* and *meta* placements of the allyl groups (aSA vs a3HBA) result in very similar cross-link densities, which are lower than that of the network with *para* placements of allyl groups (using a4HBA). Upon increasing the functionality (number of functional groups, f_{allyl}) to 3 and 4, the cross-link density remained fairly consistent with that of the a4HBA network (compare values of the a4HBA, aGenA, and aGalA networks in Figure 6a). We note that although conversion of functional groups was high in all the networks (in the range of 82−97% in our study; Tables S2−S7), they did not achieve complete conversion; however, the trends observed in the cross-link density are not explained by minor differences in functional group conversion (Table S20).

The glass transition temperatures (T_g) of thiol−ene networks (prepared following the protocol in Table 1) were explored through differential scanning calorimetry (DSC). Measurements obtained on multiple independently prepared specimens are summarized in Tables S13−S15. The T_g values measured upon the first and second heating scans were comparable to one another, within the error of the measurement. The average and standard deviation values obtained during the first heating scan are provided in Figure 6b and Table S16. The T_g's of all networks were lower than room temperature, as is often observed in thiol−ene networks, which contain flexible thioether linkages.[44] First, we will compare the networks derived from difunctional allylated phenolic acids (aSA, a3HBA, and a4HBA). The a4HBA network exhibited the highest T_g, attributed to the high cross-link density of this network (Figure 6c). Though the aSA and a3HBA networks had similar cross-link densities, the T_g of the aSA network was significantly higher than that of the a3HBA network (Figure 6c). Differences

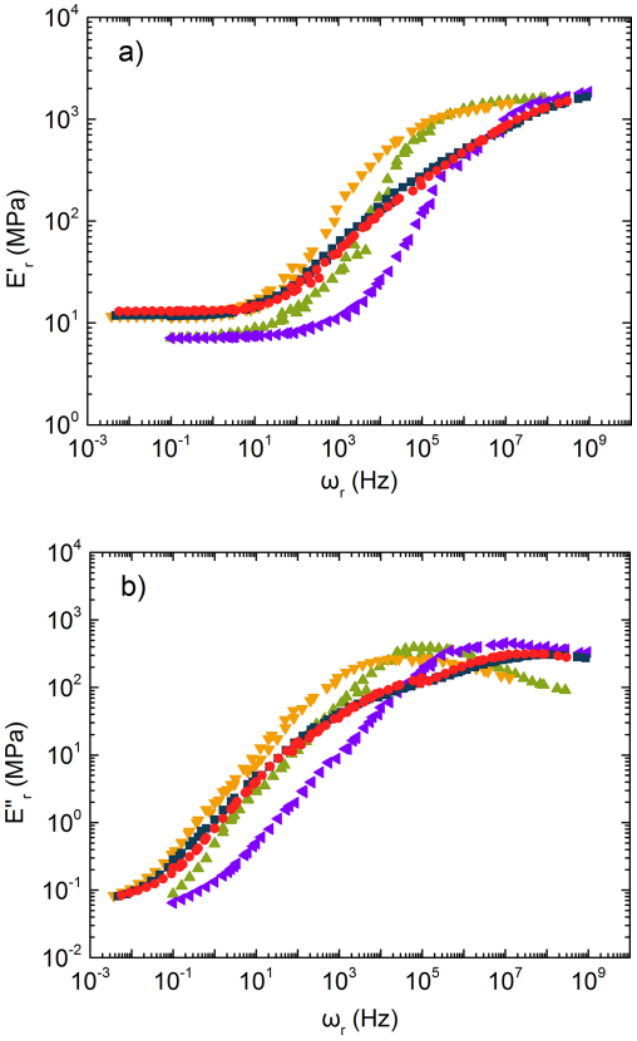

Figure 4. Master curves for the reduced (a) storage modulus (E'_r) and (b) loss modulus (E''_r) of thiol−ene networks derived from aSA (green ▲), a3HBA (purple ◀), a4HBA (yellow ▼), aGenA (dark blue ■), and aGalA (red ●). Reference temperature for time−temperature superposition was 30 °C. Data obtained on aSA and a4HBA networks were previously reported in ref 22.

in the aSA and a3HBA network T_g's may possibly be explained by differences in steric hindrance resulting from the relative placements of the allyl groups around the aromatic ring in the allylated monomer (*ortho* vs *meta* positions). Next, we examine the effect of increasing the functionality of the allylated phenolic acid on the network T_g. The aGenA and aGalA networks, derived from the allylated phenolic acids with the highest functionalities, exhibited high cross-link densities (comparable to the a4HBA network), yet low T_g values (comparable to the a3HBA network; Figure 6c). However, these networks were all prepared at stoichiometric compositions (i.e., equal concentrations of allyl and thiol groups; Table 1). As the functionality of the allylated phenolic acid increased, the molar concentration of allylated phenolic acid used to prepare the network (required for stoichiometric balance with the multifunctional thiol PETMP) thus decreased. We hypothesize that the presence of the aromatic rings on the allylated phenolic acids increases the glass transition of the networks. Thus, decreasing the molar concentration of aromatic rings throughout the network (through decreasing the

DOI: 10.1021/acs.macromol.6b01018
Macromolecules 2016, 49, 7737−7748

concentration of allylated monomer) resulted in reduction of the T_g.

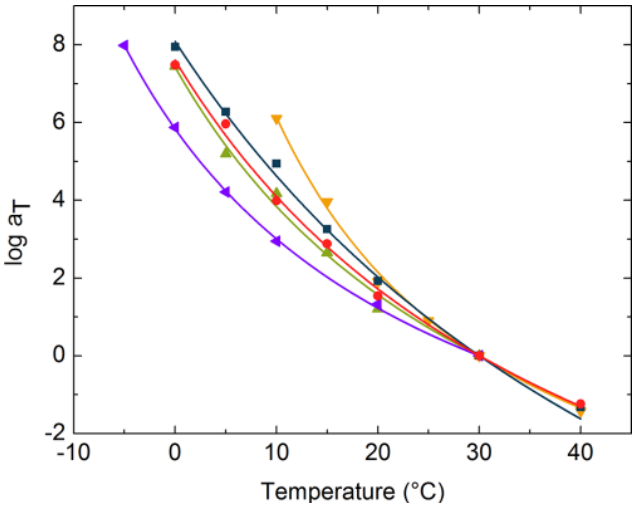

Figure 5. Temperature-dependent shift factor, a_T, for thiol−ene networks derived from aSA (green ▲), a3HBA (purple ◀), a4HBA (yellow ▼), aGenA (dark blue ■), and aGalA (red ●). Curves indicate the fit of the WLF equation to the data (for aSA, green curve: C_1 = 9.64 and C_2 = 82.47 K; for a3HBA, purple curve: C_1 = 6.599 and C_2 = 63.93 K; for a4HBA, yellow curve: C_1 = 5.85 and C_2 = 53.15 K; for aGenA, solid dark blue curve: C_1 = 16.27 and C_2 = 90.35 K; for aGalA, solid red curve: C_1 = 10.69 and C_2 = 72.18 K). Data obtained on aSA and a4HBA networks were previously reported in ref 22.

Thiol−ene networks typically exhibit sharp glass transitions, indicating a high degree of network homogeneity.[3,5−7] We observed similarly sharp transitions in the DSC and DMA data, shown in Figures S12 and S13. This is in contrast with the behavior observed in free radical and sulfur cross-linked networks with greater levels of inhomogeneity.[45−49] The aSA, a3HBA, and a4HBA networks exhibited glass transitions with similarly narrow widths (Table 3), indicating comparable degrees of homogeneity in the networks derived from difunctional allylated phenolic acids, regardless of the placement of functional groups (*ortho*, *meta*, *para*). As the functionality of the allylated phenolic acid was increased to 3 (aGenA) and 4 (aGalA), the T_g width increased, presumably indicating the formation of less homogeneous networks. Similarly, two peaks were observed in the DMA data for aGalA and aGenA networks (Figure S12), providing further evidence of increased heterogeneity in those networks.

Tensile testing was employed to probe the mechanical behavior of the thiol−ene networks. Tensile experiments were conducted on multiple specimens for each network type (reported in Figure 7a and Figures S14−S16); the average values of relevant parameters are shown in Table S17. The data in Figure 7a were fit to the ideal elastomer (affine network) model, described by[43]

$$\sigma = \frac{E}{3}\left(\lambda - \frac{1}{\lambda^2}\right) \tag{7}$$

where λ is the stretch ratio ($\lambda = 1 + \varepsilon$, where ε is the strain) and E is the tensile modulus (Young's modulus). Figure 7b shows a plot of the tensile data, formatted to highlight consistency with the ideal elastomer model. The data are consistent with the ideal elastomer model and low to moderate strains for all five

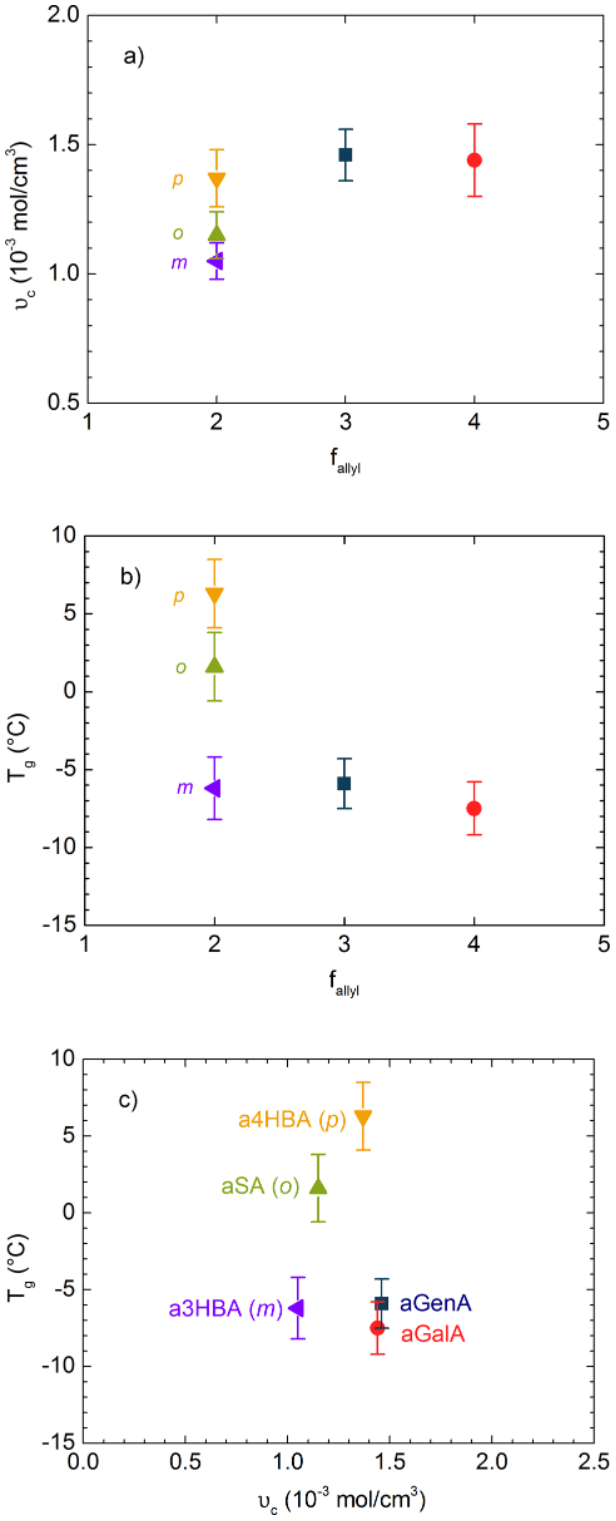

Figure 6. (a) Cross-link density (υ_c) and (b) glass transition temperature (T_g) of thiol−ene networks derived from aSA (green ▲), a3HBA (purple ◀), a4HBA (yellow ▼), aGenA (dark blue ■), and aGalA (red ●), where f_{allyl} is the functionality (number of allyl groups) of the allylated phenolic acid used to prepare the thiol−ene network. *o*, *m*, and *p* designations on the plot indicate networks derived from the *o*-, *m*-, and *p*-hydroxybenzoic acids (f_{allyl} = 2), respectively. In (c) T_g is plotted as a function of υ_c. The standard deviations on these plots indicate error characterized through multiple

DOI: 10.1021/acs.macromol.6b01018
Macromolecules 2016, 49, 7737−7748

Figure 6. continued

measurements obtained on multiple independently prepared specimens. All data are summarized in Tables S8–S16.

Table 3. Homogeneity of Thiol–Ene Networks Derived from Allylated Phenolic Acids[a]

allylated phenolic acid	f_{allyl}[b]	T_g width (°C) from DMA[c]	T_g width (°C) from DSC[d]
aSA[e]	2 (*o*)	9.6	5.8 ± 0.9
a3HBA	2 (*m*)	10.7	6.1 ± 0.3
a4HBA[e]	2 (*p*)	10.0	6.3 ± 0.5
aGenA	3	19.4	15.7 ± 0.8
aGalA	4	17.1	14.5 ± 0.9

[a]Samples were prepared following the protocol in Table 1. [b]f_{allyl} is the functionality (number of allyl groups) of the allylated phenolic acid used to prepare the thiol–ene network. [c]Full width at half-maximum of peak observed in tan δ as a function of temperature (Figure S12). [d]Difference of the onset and endset temperatures (Figure S13). [e]Data obtained on SA and 4HBA networks were previously reported in ref 22.

types of thiol–ene networks. At higher strains, in the vicinity of the elongation at break, some of the networks (a4HBA, aGenA, and aGalA) exhibited a positive deviation from the ideal network model (at a given strain, stress was higher than predicted).

A Mooney–Rivlin plot is traditionally used to identify nonideal behavior in networks. The Mooney–Rivlin model is defined as[50,51]

$$\frac{\sigma}{\lambda - \frac{1}{\lambda^2}} = 2C_1 + \frac{2C_2}{\lambda} \tag{8}$$

where C_1 and C_2 are empirical constants. In the case of an ideal network, C_2 is equal to 0. The tensile data are plotted in the Mooney–Rivlin format, as shown in Figure 7c. The behaviors of both the SA and 3HBA networks were consistent with the ideal elastomer model, resulting in a Mooney–Rivlin coefficient C_2 of close to 0 over the entire strain range, for all specimens that were tested (Table S18). The other networks (a4HBA, aGalA, and aGenA) were also consistent with the ideal elastomer model (and C_2 was close to 0) at low to moderate strains. As the strain was increased, the Mooney–Rivlin plots for the a4HBA, aGalA, and aGenA networks exhibited a negative slope (and negative value of C_2 reported in Table S18). Networks traditionally exhibit strain softening at low to moderate strains, observed as a positive slope in the Mooney–Rivlin plot, attributed to trapped entanglements and described by models that account for topological constraints.[52−54] The tensile behavior of the thiol–ene networks examined here is not consistent with trapped entanglements but is similar to that reported previously for spatially homogeneous gels[55,56] and end-linked poly(dimethylsiloxane) networks.[57] At higher strain values, the deviations from the ideal network model observed in Figure 7 for the a4HBA, aGalA, and aGenA networks (showing a negative slope in Figure 7c) are indicative of strain hardening of the networks. Strain hardening is usually observed under two conditions: (1) strain-induced crystallization of the network[58] or (2) deviation from Gaussian strand conformations in the network[59] (both typically observed at much higher strain values than were achieved in Figure 7).

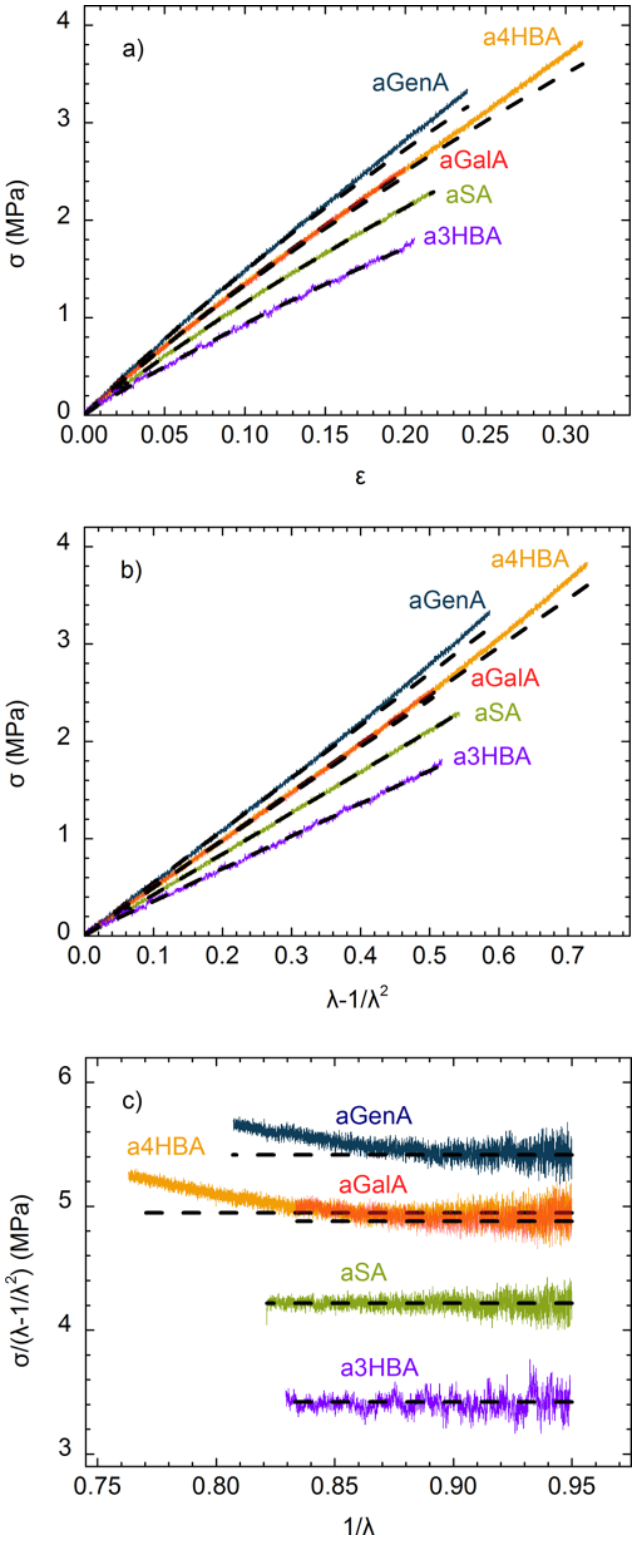

Figure 7. (a) Representative data showing tensile stress (σ) as a function of strain (ε); (b) tensile data plotted to highlight consistency with the ideal elastomer model (eq 7), where λ is the stretch ratio; and (c) tensile data plotted in the Mooney–Rivlin format (following eq 8). In all figures the solid curves indicate data obtained from thiol–ene networks derived from aSA (green), a3HBA (purple), a4HBA (yellow), aGenA (dark blue), and aGalA (red). The dashed black curves indicate the fit of the ideal elastomer model eq 7 to the data. Data were obtained on multiple independent specimens of each

DOI: 10.1021/acs.macromol.6b01018
Macromolecules 2016, 49, 7737–7748

Figure 7. continued

sample type, and all tensile data are shown in Figures S14–S16 (for a3HBA, aGenA, and aGalA). Data obtained on aSA and a4HBA networks were previously reported in ref 22. In (c), the parameters extracted from the fit of eq 8 to the data are shown in Table S18 and reported in ref 22. Data obtained at $1/\lambda > 0.95$ were not included in (c), based on uncertainties in the tensile testing measurements at these strain values ($\varepsilon < 0.05$).[60]

The ideal elastomer model (of an affine network) makes the following assumptions regarding the structure of the network: all elastic chains in the network have the same length, all cross-link junctions have the same functionality, the network is homogeneous, and each effective elastic chain obeys Gaussian statistics.[43,61] Thiol–ene chemistry traditionally results in networks of high conversion of functional groups (in the range of 82–97% in our study; Tables S2–S7) and sharp glass transitions (Table 3), generally taken to be an indication of the high degree of homogeneity of the network. The agreement with the ideal elastomer model (and fit with the Mooney–Rivlin equation with C_2 close to 0) implies a lack of heterogeneities such as dangling ends and trapped entanglements in these networks.[47,62] However, there is one important inconsistency observed in fitting the model to the data. The molecular weight between cross-links (M_c) can be readily calculated from the cross-link density ($M_c = \rho/\upsilon_c$) (in the range of 800–1100 g/mol, Table S19). If we consider a perfect network (without any defects), then we can calculate the molecular weight between junctions in the network using the chemical structure of the network (in the range of 200–500 g/mol, Table S20 and Figure S17). The experimental M_c is significantly higher than the predicted M_c for all networks (differing by factors of 2 and 4 for networks derived from difunctional [aSA, a3HBA, a4HBA] and multifunctional [aGenA, aGalA] allylated phenolic acids, respectively). Similarly, the experimental cross-link densities of all networks are lower than the theoretical predictions (Tables S19 and

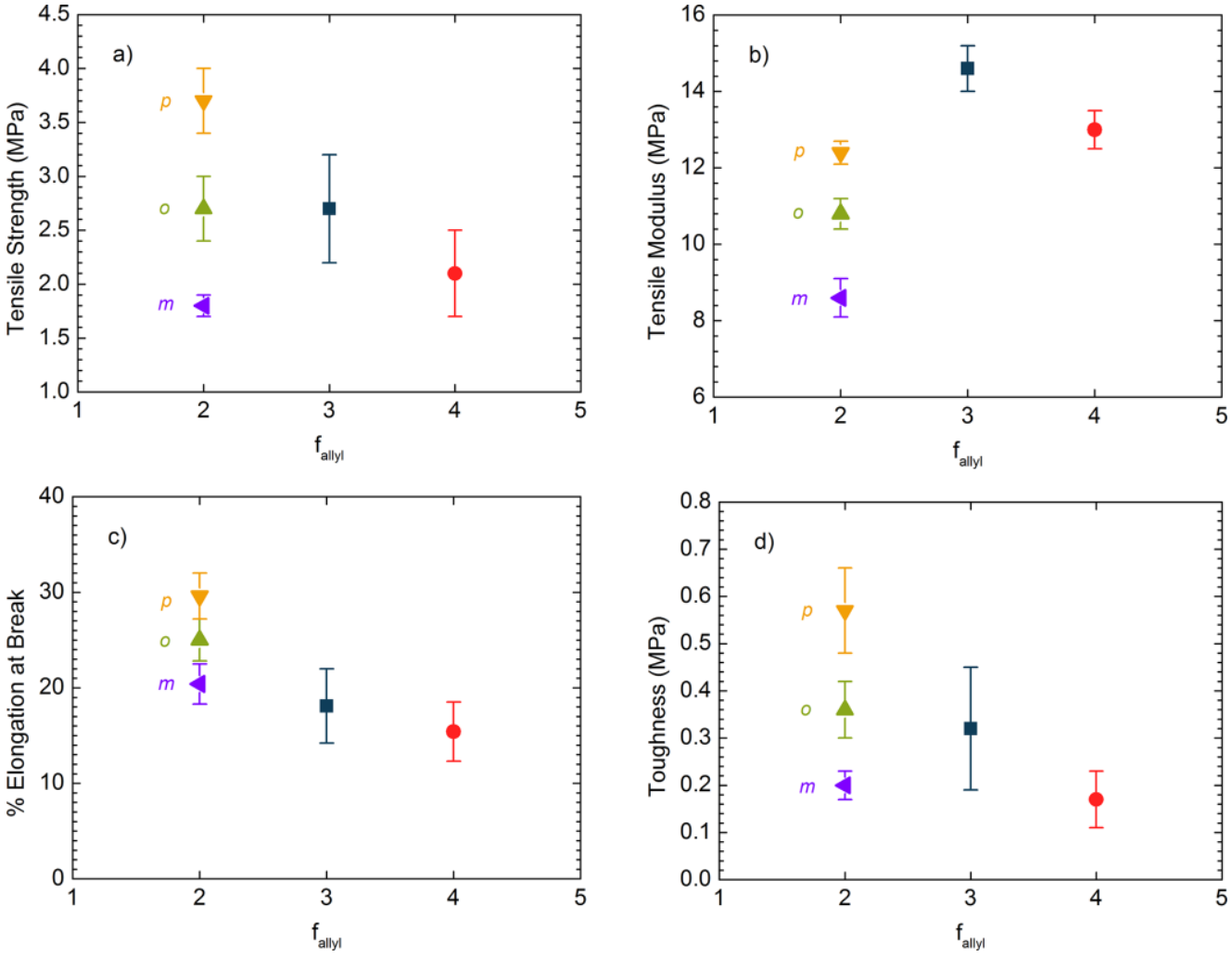

Figure 8. (a) Tensile strength, (b) tensile modulus, (c) % elongation at break, and (d) tensile toughness for thiol–ene networks derived from aSA (green ▲), a3HBA (purple ◀), a4HBA (yellow ▼), aGenA (dark blue ■) and aGalA (red ●), where f_{allyl} is the functionality (number of allyl groups) of the allylated phenolic acid used to prepare the thiol–ene network. *o*, *m*, and *p* designations on the plot indicate networks derived from the *o*-, *m*-, and *p*-hydroxybenzoic acids ($f_{allyl} = 2$), respectively. The standard deviations on these plots indicate error characterized through multiple measurements obtained on multiple independently prepared specimens (Table S17). Data obtained on aSA and a4HBA networks were previously reported in ref 22. The tensile parameters plotted as a function of the cross-link density are shown in Figure S18.

DOI: 10.1021/acs.macromol.6b01018
Macromolecules 2016, 49, 7737–7748

S20). We hypothesize that primary loop formation[63−65] may be significant in these networks, thereby increasing M_c and decreasing both υ_c and the modulus.

The tensile properties of the thiol−ene networks were characterized using measurements conducted on multiple test bars prepared from multiple independently prepared specimens (Figure 8 and Table S17). In the networks prepared from difunctional allylated phenolic acids, the a4HBA network (*para* position) exhibited the highest tensile modulus (Figure 8) and associated cross-link density (Figure 6), following by the aSA (*ortho*) and then a3HBA (*meta*) networks. The a4HBA network also exhibited the highest elongation at break, tensile strength, and tensile toughness compared to the a3HBA and aSA networks (Figure 8). We previously attributed differences in the mechanical properties of the aSA and a4HBA networks to microscopic changes in the network which impact alignment, rotation, displacement, and stretching of bonds, which are likely to be impacted by the placement of the allyl groups around the ring (*ortho*, *meta*, *para*).[22] Here we can conclude that both *meta* and *ortho* placements are less favorable arrangements of functional groups as compared to the *para* placement. In the case of networks derived from multifunctional phenolic acids (aGenA and aGalA), the high tensile modulus and low elongation at break and toughness may be attributed to two factors: the high cross-link density (Figures 6) and increased heterogeneity (evidenced by the higher glass transition width in Table 3) of the networks.

CONCLUSIONS

Biobased phenolic acids (found in plant sources) were allylated and subsequently reacted with a multifunctional thiol (in a photoinitiated reaction) to form networks. A series of phenolic acids were explored in which the relative number (2−4) and placement (*ortho*, *meta*, *para*) of functional groups was varied. The networks derived from difunctional allylated phenolic acids exhibited narrow glass transitions (indicating a high degree of network homogeneity) and glass transition temperatures (T_g) which correlated with their cross-link density. The *para* placement of allyl groups on the allylated phenolic acid produced a network with the highest cross-link density, T_g, modulus, tensile strength, and elongation at break (followed by *ortho* and then *meta*). These variations in thermal and mechanical behavior were attributed to differences in the cross-link densities of the networks as well as microscopic changes in the network upon deformation, which are likely impacted by the placement of functional groups around the aromatic ring. As the functionality of the allylated monomer increased (to 3−4 allyl groups per molecule), the cross-link density remained high yet the T_g decreased, attributed to a lower concentration of aromatic rings throughout the network structure (as all networks were prepared at the stoichiometric ratio of allyl and thiol functional groups). The networks derived from the higher functionality allylated phenolic acids also exhibited lower elongation at break and associated tensile strength and tensile toughness, likely due to increased heterogeneity of the networks (indicated by higher glass transition widths compared to the networks derived from difunctional allylated phenolic acids). All networks exhibited behavior consistent with an ideal elastomer (affine network) at low to moderate strains, albeit with lower moduli than predicted from the monomer chemical structure. At the high end of the strain ranges achieved, some of the networks exhibited strain hardening behavior, in which the stress at a given strain was higher than that predicted for an ideal elastomer.

ASSOCIATED CONTENT

Supporting Information

The Supporting Information is available free of charge on the ACS Publications website at DOI: 10.1021/acs.macromol.6b01018.

NMR spectra obtained on the phenolic acids and allylated phenolic acids, including ^{1}H NMR, ^{13}C NMR, DEPT 45, 90, 135, COSY, HSQC, and HMBC (Figures S1−S6); synthetic schemes for photoinitiated thiol−ene reaction between allylated phenolic acids and PETMP (Scheme S1); FTIR spectra obtained before and after curing (Figure S7); assignment of FTIR vibrational modes (Table S1); thiol−ene reaction conversion quantified through FTIR (Tables S2−S7); FTIR peak intensities and glass transition temperatures as functions of isothermal postcure time (Figures S8 and S9); storage and loss moduli as a function of strain (Figure S10) and frequency (Figure S11) determined through DMA; cross-link density determined from DMA using repeat measurements on various specimens (Tables S8−S12); glass transition temperatures determined through DSC using repeat measurements on various specimens (Tables S13−S15); average and standard deviation of glass transition and thermal degradation temperatures (Table S16); tan δ vs temperature measured through DMA (Figure S12) and raw DSC data (Figure S13) showing width of the glass transition; stress−strain curves for each specimen measured and included in the average values of the tensile parameters reported (Figures S14−S16); average and standard deviations of tensile properties (Table S17); parameters extracted from fit of Mooney−Rivlin equation to the tensile data (Table S18); calculation of molecular weight between cross-links using the DMA modulus and theoretical predictions (Table S19 and Figure S17); and tensile parameters as functions of the cross-link density (Figure S18) (PDF)

AUTHOR INFORMATION

Corresponding Author

*E-mail mlrobertson@uh.edu; Tel 713-743-2748 (M.L.R.).

Notes

The authors declare no competing financial interest.

ACKNOWLEDGMENTS

The authors acknowledge financial support from the National Science Foundation (CMMI-1334838 (M.L.R.) and CHE-1410272 (K.L.W.)), the Norman Hackerman Advanced Research Program of the Texas Higher Education Coordinating Board (003652-0022-2013, M.L.R.), the University of Houston (M.L.R.), and the Welch Foundation (A-0001, K.L.W.). The authors thank Ramanan Krishnamoorti, Brian Rohde, and Daehak Kim (University of Houston) for access, training, and data analysis on the FTIR and TGA instruments. We thank Hiruy Tesefay (University of Houston) for assistance with monomer synthesis and purification. We appreciate the assistance of Charles Anderson for access and training in the University of Houston Department of Chemistry Nuclear Magnetic Resonance Facility. We appreciate the contribution of Haleh Ardebili and Mejdi Kammoun (University of Houston)

DOI: 10.1021/acs.macromol.6b01018
Macromolecules 2016, 49, 7737−7748

for access and training on the DMA instrument. We thank Bradley D. Olsen and Rui Wang (Massachusetts Institute of Technology) for helpful discussions regarding primary loop formation in networks. We appreciate the advice and assistance of Shu Wang, Avantika Singh, and Vivek Yadav (University of Houston).

REFERENCES

(1) Wilbon, P. A.; Chu, F.; Tang, C. Progress in Renewable Polymers from Natural Terpenes, Terpenoids, and Rosin. *Macromol. Rapid Commun.* **2013**, *34* (1), 8−37.
(2) Gandini, A. The irruption of polymers from renewable resources on the scene of macromolecular science and technology. *Green Chem.* **2011**, *13* (5), 1061−1083.
(3) Hoyle, C. E.; Lee, T. Y.; Roper, T. Thiol−enes: Chemistry of the past with promise for the future. *J. Polym. Sci., Part A: Polym. Chem.* **2004**, *42* (21), 5301−5338.
(4) Lu, H.; Carioscia, J. A.; Stansbury, J. W.; Bowman, C. N. Investigations of step-growth thiol-ene polymerizations for novel dental restoratives. *Dent. Mater.* **2005**, *21* (12), 1129−1136.
(5) Hoyle, C. E.; Bowman, C. N. Thiol−Ene Click Chemistry. *Angew. Chem., Int. Ed.* **2010**, *49* (9), 1540−1573.
(6) Kade, M. J.; Burke, D. J.; Hawker, C. J. The power of thiol-ene chemistry. *J. Polym. Sci., Part A: Polym. Chem.* **2010**, *48* (4), 743−750.
(7) Li, Q.; Zhou, H.; Wicks, D. A.; Hoyle, C. E. Thiourethane-based thiol-ene high Tg networks: Preparation, thermal, mechanical, and physical properties. *J. Polym. Sci., Part A: Polym. Chem.* **2007**, *45* (22), 5103−5111.
(8) Samuelsson, J.; Jonsson, M.; Brinck, T.; Johansson, M. Thiol-ene coupling reaction of fatty acid monomers. *J. Polym. Sci., Part A: Polym. Chem.* **2004**, *42* (24), 6346−6352.
(9) Black, M.; Rawlins, J. W. Thiol−ene UV-curable coatings using vegetable oil macromonomers. *Eur. Polym. J.* **2009**, *45* (5), 1433−1441.
(10) Chen, Z.; Chisholm, B.; Patani, R.; Wu, J.; Fernando, S.; Jogodzinski, K.; Webster, D. Soy-based UV-curable thiol−ene coatings. *J. Coat. Technol. Res.* **2010**, *7* (5), 603−613.
(11) Lligadas, G.; Ronda, J. C.; Galià, M.; Cádiz, V. Monomers and polymers from plant oils via click chemistry reactions. *J. Polym. Sci., Part A: Polym. Chem.* **2013**, *51* (10), 2111−2124.
(12) Türünç, O.; Meier, M. A. R. The thiol-ene (click) reaction for the synthesis of plant oil derived polymers. *Eur. J. Lipid Sci. Technol.* **2013**, *115* (1), 41−54.
(13) Acosta Ortiz, R.; Martinez, A. Y. R.; García Valdez, A. E.; Berlanga Duarte, M. L. Preparation of a crosslinked sucrose polymer by thiol−ene photopolymerization using dithiothreitol as comonomer. *Carbohydr. Polym.* **2010**, *82* (3), 822−828.
(14) Ortiz, R. A.; Garcia Valdéz, A. E.; Martinez Aguilar, M. G.; Berlanga Duarte, M. L. An effective method to prepare sucrose polymers by Thiol-Ene photopolymerization. *Carbohydr. Polym.* **2009**, *78* (2), 282−286.
(15) Hearon, K.; Nash, L. D.; Rodriguez, J. N.; Lonnecker, A. T.; Raymond, J. E.; Wilson, T. S.; Wooley, K. L.; Maitland, D. J. A High-Performance Recycling Solution for Polystyrene Achieved by the Synthesis of Renewable Poly(thioether) Networks Derived from d-Limonene. *Adv. Mater.* **2014**, *26* (10), 1552−1558.
(16) Link, L. A.; Lonnecker, A. T.; Hearon, K.; Maher, C. A.; Raymond, J. E.; Wooley, K. L. Photo-cross-linked poly(thioether-co-carbonate) networks derived from the natural product quinic acid. *ACS Appl. Mater. Interfaces* **2014**, *6* (20), 17370−5.
(17) Fertier, L.; Koleilat, H.; Stemmelen, M.; Giani, O.; Joly-Duhamel, C.; Lapinte, V.; Robin, J.-J. The use of renewable feedstock in UV-curable materials − A new age for polymers and green chemistry. *Prog. Polym. Sci.* **2013**, *38* (6), 932−962.
(18) Russell, W. R.; Labat, A.; Scobbie, L.; Duncan, G. J.; Duthie, G. G. Phenolic acid content of fruits commonly consumed and locally produced in Scotland. *Food Chem.* **2009**, *115* (1), 100−104.
(19) Manach, C.; Scalbert, A.; Morand, C.; Rémésy, C.; Jiménez, L. Polyphenols: food sources and bioavailability. *Am. J. Clin. Nutr.* **2004**, *79* (5), 727−747.
(20) Schieber, A.; Stintzing, F. C.; Carle, R. By-products of plant food processing as a source of functional compounds — recent developments. *Trends Food Sci. Technol.* **2001**, *12* (11), 401−413.
(21) Naczk, M.; Shahidi, F. Phenolics in cereals, fruits and vegetables: Occurrence, extraction and analysis. *J. Pharm. Biomed. Anal.* **2006**, *41* (5), 1523−1542.
(22) Yang, G.; Kristufek, S. L.; Link, L. A.; Wooley, K. L.; Robertson, M. L. Synthesis and Physical Properties of Thiol−Ene Networks Utilizing Plant-Derived Phenolic Acids. *Macromolecules* **2015**, *48* (23), 8418−8427.
(23) Aouf, C.; Nouailhas, H.; Fache, M.; Caillol, S.; Boutevin, B.; Fulcrand, H. Multi-functionalization of gallic acid. Synthesis of a novel bio-based epoxy resin. *Eur. Polym. J.* **2013**, *49* (6), 1185−1195.
(24) Pascault, J.-P.; Sautereau, H.; Verdu, J.; Williams, R. J. J. *Thermosetting Polymers*; Marcel Dekker, Inc.: New York, 2002.
(25) Ewing, W. W.; Mikovsky, R. J. Calcium Nitrate. V. Partial Molal Volumes of Water and Calcium Nitrate in Concentrated Solutions. *J. Am. Chem. Soc.* **1950**, *72* (3), 1390−1393.
(26) Brown, D. P.; Duong, H. Q. Synthesis of Novel Aromatic Macrolactones via Ring Closing Metathesis of Substituted Phenylalkanoic Acid Allylic Esters. *J. Heterocycl. Chem.* **2008**, *45*, 435.
(27) Yi, B.; Long, S.; Gonzalez-Cestari, T. F.; Henderson, B. J.; Pavlovicz, R. E.; Werbovetz, K.; Li, C.; McKay, D. B. Discovery of benzamide analogs as negative allosteric modulators of human neuronal nicotinic receptors: pharmacophore modeling and structure-activity relationship studies. *Bioorg. Med. Chem.* **2013**, *21* (15), 4730−43.
(28) Murakami, H.; Minami, T.; Ozawa, F. Facile and Selective Deallylation of Allyl Ethers Using Diphosphinidenecyclobutene-Coordinated Palladium Catalysts. *J. Org. Chem.* **2004**, *69*, 4482.
(29) TAKAC, M. J.-M.; TOPIC, D. V. FT-IR and NMR spectroscopic studies of salicylic acid derivatives. II. Comparison of 2-hydroxy- and 2,4- and 2,5-dihydroxy derivatives. *Acta Pharm.* **2004**, *54*, 177.
(30) Rzokee, A. A.; Ahmad, A. Synthesis, spectroscopic studies and thermal analysis of charge-transfer complex of 2,2′-bipyridine with 4-hydroxybenzoic acid in different polar solvents. *J. Mol. Struct.* **2014**, *1076*, 453−460.
(31) Cox, R. H. Proton magnetic resonance spectra of mono-substituted benzoic acids. *Spectrochimica Acta Part A: Molecular Spectroscopy* **1969**, *25* (7), 1189−1194.
(32) Cramer, N. B.; Reddy, S. K.; O'Brien, A. K.; Bowman, C. N. Thiol−Ene Photopolymerization Mechanism and Rate Limiting Step Changes for Various Vinyl Functional Group Chemistries. *Macromolecules* **2003**, *36* (21), 7964−7969.
(33) Silverstein, R. M.; Webster, F. X.; Kiemle, D. *Spectrometric Identification of Organic Compounds*, 7th ed.; John Wiley & Sons: Hoboken, NJ, 2005.
(34) Claudino, M.; van der Meulen, I.; Trey, S.; Jonsson, M.; Heise, A.; Johansson, M. Photoinduced thiol-ene crosslinking of globalide/ε-caprolactone copolymers: Curing performance and resulting thermoset properties. *J. Polym. Sci., Part A: Polym. Chem.* **2012**, *50* (1), 16−24.
(35) Shigetomi, Y.; Ono, N.; Kato, H.; Oki, M. Allylic Polymers IV. The Effect of Alkyl-Substituents on Copolymerization of Allyl Alkyl Ethers with Vinyl Acetate. *Polym. J.* **1992**, *24* (3), 247−255.
(36) Scheier, L. Salicylic Acid: One More Reason to Eat Your Fruits and Vegetables. *J. Am. Diet. Assoc.* **2001**, *101* (12), 1406−1408.
(37) Dey, G.; Chakraborty, M.; Mitra, A. Profiling C6-C3 and C6-C1 phenolic metabolites in Cocos nucifera. *J. Plant Physiol.* **2005**, *162* (4), 375−81.
(38) Griffiths, L. A. Occurrence of Gentisic Acid in Plant Tissues. *Nature* **1958**, *182*, 733−734.
(39) Reynolds, L. D.; Wilson, N. G. *Scribes and Scholars*, 3rd ed.; Oxford: 1991.
(40) Dealy, J.; Plazek, D. Temperature-Time Superposition - A User Guide. *Rheol. Bull.* **2009**, *78* (2), 16−31.

DOI: 10.1021/acs.macromol.6b01018
Macromolecules 2016, 49, 7737−7748

(41) Malkin, A. Y.; Isayev, A. I. *Rheology - Concepts, Methods, & Applications*; ChemTec Publishing: Toronto, 2006.
(42) Williams, M. L.; Landel, R. F.; Ferry, J. D. The Temperature Dependence of Relaxation Mechanisms in Amorphous Polymers and Other Glass-forming Liquids. *J. Am. Chem. Soc.* **1955**, *77* (14), 3701−3707.
(43) Flory, P. J. *Principles of Polymer Chemistry*; Cornell University Press: Ithaca, NY, 1953.
(44) Li, Q.; Zhou, H.; Wicks, D. A.; Hoyle, C. E. Thiourethane-based thiol-ene highTg networks: Preparation, thermal, mechanical, and physical properties. *J. Polym. Sci., Part A: Polym. Chem.* **2007**, *45* (22), 5103−5111.
(45) Kannurpatti, A. R.; Anseth, J. W.; Bowman, C. N. A study of the evolution of mechanical properties and structural heterogeneity of polymer networks formed by photopolymerizations of multifunctional (meth)acrylates. *Polymer* **1998**, *39* (12), 2507−2513.
(46) Senyurt, A. F.; Wei, H.; Hoyle, C. E.; Piland, S. G.; Gould, T. E. Ternary Thiol−Ene/Acrylate Photopolymers: Effect of Acrylate Structure on Mechanical Properties. *Macromolecules* **2007**, *40* (14), 4901−4909.
(47) Shibayama, M. Spatial inhomogeneity and dynamic fluctuations of polymer gels. *Macromol. Chem. Phys.* **1998**, *199* (1), 1−30.
(48) Kannurpatti, A. R.; Anderson, K. J.; Anseth, J. W.; Bowman, C. N. Use of "living" radical polymerizations to study the structural evolution and properties of highly crosslinked polymer networks. *J. Polym. Sci., Part B: Polym. Phys.* **1997**, *35* (14), 2297−2307.
(49) Ikeda, Y.; Higashitani, N.; Hijikata, K.; Kokubo, Y.; Morita, Y.; Shibayama, M.; Osaka, N.; Suzuki, T.; Endo, H.; Kohjiya, S. Vulcanization: New Focus on a Traditional Technology by Small-Angle Neutron Scattering. *Macromolecules* **2009**, *42* (7), 2741−2748.
(50) Mooney, M. A Theory of Large Elastic Deformation. *J. Appl. Phys.* **1940**, *11* (9), 582−592.
(51) Rivlin, R. S. The Elasticity of Rubber. *Rubber Chem. Technol.* **1992**, *65* (3), 51−66.
(52) Rubinstein, M.; Panyukov, S. Nonaffine Deformation and Elasticity of Polymer Networks. *Macromolecules* **1997**, *30* (25), 8036−8044.
(53) Rubinstein, M.; Panyukov, S. Elasticity of Polymer Networks. *Macromolecules* **2002**, *35* (17), 6670−6686.
(54) Edwards, S. F. Statistical Mechanics of Polymerized Material. *Proc. Phys. Soc., London* **1967**, *92* (575P), 9−16.
(55) Akagi, Y.; Katashima, T.; Katsumoto, Y.; Fujii, K.; Matsunaga, T.; Chung, U.-i.; Shibayama, M.; Sakai, T. Examination of the Theories of Rubber Elasticity Using an Ideal Polymer Network. *Macromolecules* **2011**, *44* (14), 5817−5821.
(56) Oshima, K.; Fujimoto, T.; Minami, E.; Mitsukami, Y. Model Polyelectrolyte Gels Synthesized by End-Linking of Tetra-Arm Polymers with Click Chemistry: Synthesis and Mechanical Properties. *Macromolecules* **2014**, *47* (21), 7573−7580.
(57) Mark, J. E.; Tang, M. Y. Dependence of the elastomeric properties of bimodal networks on the lengths and amounts of the short chains. *J. Polym. Sci., Polym. Phys. Ed.* **1984**, *22* (11), 1849−1855.
(58) Trabelsi, S.; Albouy, P. A.; Rault, J. Crystallization and Melting Processes in Vulcanized Stretched Natural Rubber. *Macromolecules* **2003**, *36* (20), 7624−7639.
(59) Gordon, M. *The Physics of Rubber Elasticity*, 3rd ed.; Treloar, L. R. G., Ed.; Clarendon Press: Oxford, 1975; pp xii + 370. *Br. Polym. J.* **1976**, *8* (1), 39−39.
(60) Schlögl, S.; Trutschel, M.-L.; Chassé, W.; Riess, G.; Saalwächter, K. Entanglement Effects in Elastomers: Macroscopic vs Microscopic Properties. *Macromolecules* **2014**, *47* (9), 2759−2773.
(61) Hild, G. Model networks based on `endlinking' processes: synthesis, structure and properties. *Prog. Polym. Sci.* **1998**, *23* (6), 1019−1149.
(62) Schlogl, S.; Trutschel, M. L.; Chasse, W.; Riess, G.; Saalwachter, K. Entanglement Effects in Elastomers: Macroscopic vs Microscopic Properties. *Macromolecules* **2014**, *47* (9), 2759−2773.
(63) Zhou, H.; Woo, J.; Cok, A. M.; Wang, M.; Olsen, B. D.; Johnson, J. A. Counting primary loops in polymer gels. *Proc. Natl. Acad. Sci. U. S. A.* **2012**, *109* (47), 19119−19124.
(64) Wang, R.; Alexander-Katz, A.; Johnson, J. A.; Olsen, B. D. Universal Cyclic Topology in Polymer Networks. *Phys. Rev. Lett.* **2016**, *116* (18), 188302.
(65) Kawamoto, K.; Zhong, M.; Wang, R.; Olsen, B. D.; Johnson, J. A. Loops versus Branch Functionality in Model Click Hydrogels. *Macromolecules* **2015**, *48* (24), 8980−8988.

DOI: 10.1021/acs.macromol.6b01018
Macromolecules 2016, 49, 7737−7748